

# **Nitranilic acid hexahydrate, a novel benchmark system of the Zundel cation in an intrinsically asymmetric environment: spectroscopic features and hydrogen bond dynamics characterised by experimental and theoretical methods**

Krešimir Molčanov<sup>a</sup>, Jernej Stare<sup>\*b,c</sup>, Mikhail V. Vener<sup>d</sup>, Biserka Kojić-Prodić<sup>\*a</sup>,  
Gregor Mali<sup>b,e</sup>, Jože Grdadolnik<sup>b,e</sup>, Vlasta Mohaček-Grošev<sup>a</sup>

<sup>a</sup> Rudjer Bošković Institute, Bijenička 54, HR-10000 Zagreb, Croatia

<sup>b</sup> National Institute of Chemistry, Hajdrihova 19, SI-1000 Ljubljana, Slovenia

<sup>c</sup> Laboratory of Computational Chemistry and Biochemistry, EPFL Lausanne, Switzerland.

<sup>d</sup> Department of Quantum Chemistry, Mendeleev University of Chemical Technology, Miusskaya Square 9, 125047 Moscow, Russia

<sup>e</sup> EN-FIST Centre of Excellence, Dunajska c. 156, SI-Ljubljana, Slovenia

## **Supplementary Information**

### **Contents:**

#### **S1 Crystal structures**

#### **S2 Details on theoretical calculations**

**S2.1 Optimization of crystalline ZNATH by various programs**

**S2.2 Optimization of substituted analogs of ZNATH in the solid state**

**S2.3 Structure, NBO analysis and proton affinity of NA analogs (dianions) in the gas phase**

**S2.4 First-principle calculations of isotropic chemical shifts**

#### **S3 Spectroscopic characteristics of the nitranilate anion**

**S3.1 Infrared spectroscopy**

**S3.2 Raman spectroscopy**

## S1 Crystal structures

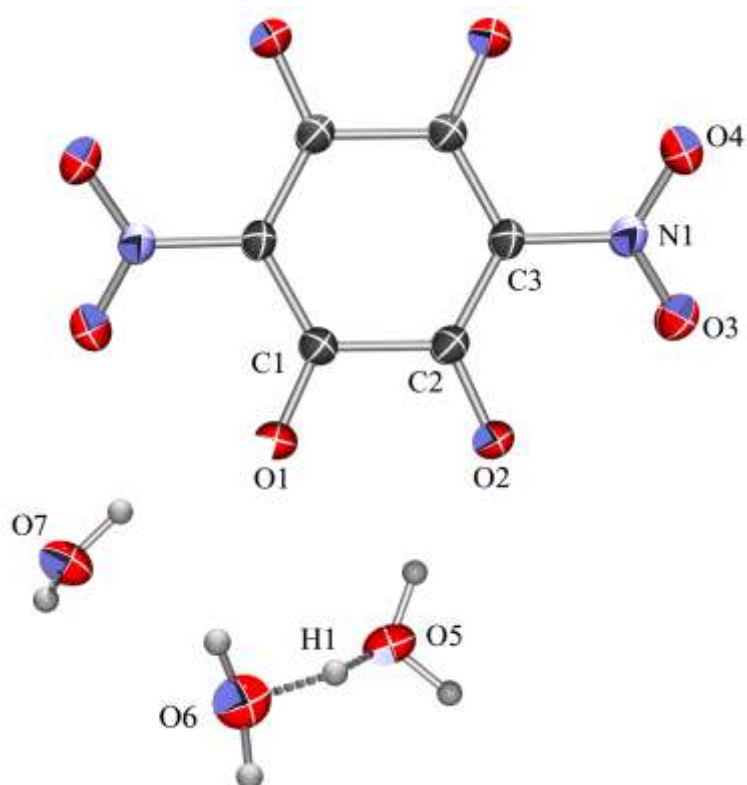


**Figure S1.1.** ORTEP-3 drawing of an asymmetric unit of ZNATH (intensity data measured at 293 K). Crystallographic symmetry of the nitranilate anion is  $C_i$ . Atomic displacement ellipsoids are drawn for the probability of 50 % and hydrogen atoms are shown as spheres of arbitrary radii.

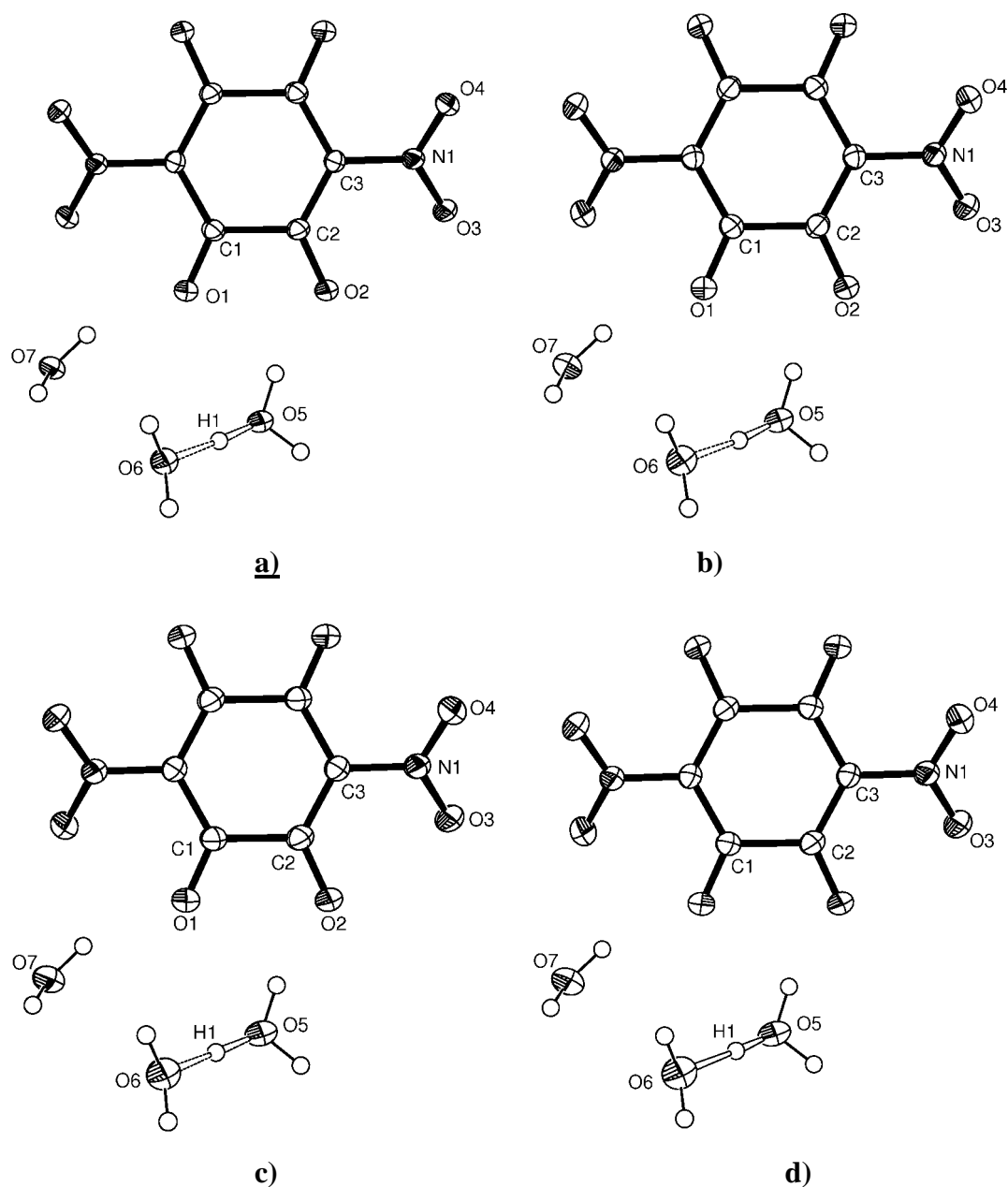


**Figure S1.2.** ORTEP-3 drawings of the asymmetric unit at a) 100 K, b) 150 K, c) 200 K and d) 250 K. Displacement ellipsoids are drawn for the probability of 50 % and hydrogen atoms are shown as spheres of arbitrary radii. Atom labeling is given in **Figure S1.1**.

**Table S1.1.** Geometric parameters of H-bonds not involving the Zundel cation.

		$D-H / \text{\AA}$	$H \cdots A / \text{\AA}$	$D \cdots A / \text{\AA}$	$D-H \cdots A / \text{\AA}$	Symm. op. on A
O7-H7A $\cdots$ O1	100 K	0.92(2)	2.04(2)	2.9214(15)	161(2)	$x, y, z$
	150 K	0.91(2)	2.05(2)	2.9281(18)	162(2)	$x, y, z$
	200 K	0.90(2)	2.07(2)	2.9372(16)	161(2)	$x, y, z$
	250 K	0.91(2)	2.07(2)	2.9456(18)	162(2)	$x, y, z$
	293 K	0.92(3)	2.08(3)	2.9597(18)	161(2)	$x, y, z$
O7-H7A $\cdots$ O4	100 K	0.92(2)	2.21(3)	2.8085(16)	122(2)	$-x, 1-y, 1-z$
	150 K	0.91(2)	2.22(3)	2.8137(17)	126(2)	$-x, 1-y, 1-z$
	200 K	0.90(2)	2.22(3)	2.8214(15)	124(2)	$-x, 1-y, 1-z$
	250 K	0.91(2)	2.23(3)	2.8288(16)	123(2)	$-x, 1-y, 1-z$
	293 K	0.92(3)	2.23(3)	2.8412(17)	124(2)	$-x, 1-y, 1-z$
O7-H7B $\cdots$ O3	100 K	0.94(3)	2.05(3)	2.9517(14)	159(3)	$-x, 1/2+y, 3/2-z$
	150 K	0.93(3)	2.07(3)	2.9630(18)	159(3)	$-x, 1/2+y, 3/2-z$
	200 K	0.93(3)	2.08(3)	2.9718(16)	162(3)	$-x, 1/2+y, 3/2-z$
	250 K	0.92(3)	2.10(3)	2.9863(18)	164(3)	$-x, 1/2+y, 3/2-z$
	293 K	0.93(3)	2.13(3)	3.0012(18)	157(3)	$-x, 1/2+y, 3/2-z$
O7-H7B $\cdots$ O4	100 K	0.94(3)	2.41(3)	3.0463(15)	125(2)	$-x, 1/2+y, 3/2-z$
	150 K	0.93(3)	2.37(3)	3.0488(17)	129(2)	$-x, 1/2+y, 3/2-z$
	200 K	0.93(3)	2.40(3)	3.0521(15)	127(3)	$-x, 1/2+y, 3/2-z$
	250 K	0.92(3)	2.38(3)	3.0576(16)	131(3)	$-x, 1/2+y, 3/2-z$
	293 K	0.93(3)	2.43(3)	3.0633(17)	126(2)	$-x, 1/2+y, 3/2-z$

**Table S1.2.** Bond lengths in the nitranilate anion. Symmetry operator:  $i) -x, 1-y, 1-z$ .

	100 K	150 K	200 K	250 K	293 K
C1 – C2	1.556(2)	1.555(2)	1.5573(19)	1.5521(19)	1.5538(19)
C2 – C3	1.415(2)	1.414(2)	1.4104(19)	1.4107(19)	1.4123(19)
C1 – C3 <sup>i</sup>	1.434(2)	1.433(2)	1.4344(18)	1.4345(18)	1.4322(18)
C1 – O1	1.2211(18)	1.2252(19)	1.2188(18)	1.2205(18)	1.2201(18)
C2 – O2	1.2386(18)	1.2376(19)	1.2380(17)	1.2403(16)	1.2368(17)
C3 – N1	1.4369(18)	1.4393(18)	1.4382(18)	1.4401(18)	1.4380(18)
N1 – O3	1.2424(17)	1.2397(18)	1.2365(16)	1.2322(16)	1.2306(17)
N1 – O4	1.2283(17)	1.2301(17)	1.2271(16)	1.2258(16)	1.2250(17)

**Table S1.3** Crystallographic, data collection and structure refinement details of ZNATH.

Compound	ZNATH, 100 K	ZNATH, 150 K	ZNATH, 200 K	ZNATH, 250 K
Empirical formula	C <sub>6</sub> H <sub>14</sub> N <sub>2</sub> O <sub>14</sub>	C <sub>6</sub> H <sub>14</sub> N <sub>2</sub> O <sub>14</sub>	C <sub>6</sub> H <sub>14</sub> N <sub>2</sub> O <sub>14</sub>	C <sub>6</sub> H <sub>14</sub> N <sub>2</sub> O <sub>14</sub>
Formula wt. / g mol <sup>-1</sup>	388.19	388.19	388.19	388.19
Color	pale orange	pale orange	pale orange	pale orange
Crystal dimensions / mm	0.22 x 0.08 x 0.06	0.22 x 0.08 x 0.06	0.22 x 0.08 x 0.06	0.30 x 0.05 x 0.04
Space group	<i>P</i> 2 <sub>1</sub> / <i>c</i>	<i>P</i> 2 <sub>1</sub> / <i>c</i>	<i>P</i> 2 <sub>1</sub> / <i>c</i>	<i>P</i> 2 <sub>1</sub> / <i>c</i>
<i>a</i> / Å	3.5823(2)	3.6004(2)	3.61610(10)	3.63560(10)
<i>b</i> / Å	19.2469(6)	19.2689(9)	19.3017(5)	19.3519(5)
<i>c</i> / Å	9.1875(4)	9.1881(5)	9.1867(2)	9.1850(2)
$\alpha$ / °	90	90	90	90
$\beta$ / °	93.540(4)	93.605(5)	93.748(2)	94.017(2)
$\gamma$ / °	90	90	90	90
<i>Z</i>	2	2	2	2
<i>V</i> / Å <sup>3</sup>	632.25(5)	636.17(6)	639.83(3)	644.63(3)
<i>D</i> <sub>calc</sub> / g cm <sup>-3</sup>	1.776	1.765	1.755	1.742
$\lambda$ / Å	1.54179 (CuK $\alpha$ )	1.54179 (CuK $\alpha$ )	1.54179 (CuK $\alpha$ )	1.54179 (CuK $\alpha$ )
$\mu$ / mm <sup>-1</sup>	1.629	1.619	1.610	1.598
$\Theta$ range / °	4.59 – 75.91	4.59 – 75.57	4.58 – 76.04	4.57 – 75.45
<i>T</i> / K	100(2)	150(2)	200(2)	250(2)
Diffractometer type	Xcalibur Nova	Xcalibur Nova	Xcalibur Nova	Xcalibur Nova
Range of <i>h</i> , <i>k</i> , <i>l</i>	-4 < <i>h</i> < 4; -24 < <i>k</i> < 15; -11 < <i>l</i> < 11	-4 < <i>h</i> < 4; -24 < <i>k</i> < 9; -11 < <i>l</i> < 11	-4 < <i>h</i> < 4; -24 < <i>k</i> < 14; -10 < <i>l</i> < 11	-3 < <i>h</i> < 4; -18 < <i>k</i> < 24; -9 < <i>l</i> < 11
Reflections collected	2728	2605	2722	2780
Independent reflections	1310	1315	1326	1335
Observed reflections ( <i>I</i> ≥ 2 $\sigma$ )	1197	1184	1197	1202
Absorption correction	Multi-scan	Multi-scan	Multi-scan	Multi-scan
<i>T</i> <sub>min</sub> , <i>T</i> <sub>max</sub>	0.3337; 1.0000	0.4649; 1.0000	0.4928; 1.0000	0.7615; 1.0000
<i>R</i> <sub>int</sub>	0.0283	0.0227	0.0247	0.0288
<i>R</i> ( <i>F</i> )	0.0404	0.0418	0.0381	0.0404
<i>R</i> <sub>w</sub> ( <i>F</i> <sup>2</sup> )	0.1126	0.1165	0.1051	0.1161
Goodness of fit	1.075	1.060	1.051	1.062
H atom treatment	Free	Free	Free	Free
No. of parameters, restraints	128, 9	128, 9	128, 9	128, 9
$\Delta\rho_{\max}$ , $\Delta\rho_{\min}$ (eÅ <sup>-3</sup> )	0.255; -0.244	0.296; -0.316	0.265; -0.238	0.243; -0.213

**Table S1.3** Cont'd.

Compound	<b>ZNATH, 293 K</b>
Empirical formula	C <sub>6</sub> H <sub>14</sub> N <sub>2</sub> O <sub>14</sub>
Formula wt. / g mol <sup>-1</sup>	388.19
Color	pale orange
Crystal dimensions / mm	0.22 x 0.08 x 0.06
Space group	<i>P</i> 2 <sub>1</sub> / <i>c</i>
<i>a</i> / Å	3.65680(10)
<i>b</i> / Å	19.4101(3)
<i>c</i> / Å	9.1903(2)
<i>α</i> / °	90
<i>β</i> / °	94.287(2)
<i>γ</i> / °	90
<i>Z</i>	2
<i>V</i> / Å <sup>3</sup>	650.49(2)
<i>D</i> <sub>calc</sub> / g cm <sup>-3</sup>	1.727
<i>λ</i> / Å	1.54179 (CuKα)
<i>μ</i> / mm <sup>-1</sup>	1.584
<i>θ</i> range / °	6.64 – 75.75
<i>T</i> / K	293(2)
Diffractometer type	Xcalibur Nova
Range of <i>h</i> , <i>k</i> , <i>l</i>	-4 < <i>h</i> < 4; -24 < <i>k</i> < 14; -10 < <i>l</i> < 11
Reflections collected	2434
Independent reflections	1321
Observed reflections ( <i>I</i> ≥ 2σ)	1228
Absorption correction	Multi-scan
<i>T</i> <sub>min</sub> , <i>T</i> <sub>max</sub>	0.7823; 1.0000
<i>R</i> <sub>int</sub>	0.0211
<i>R</i> ( <i>F</i> )	0.0456
<i>R</i> <sub>w</sub> ( <i>F</i> <sup>2</sup> )	0.1267
Goodness of fit	1.083
H atom treatment	Free
No. of parameters, restraints	128, 9
<i>Δρ</i> <sub>max</sub> , <i>Δρ</i> <sub>min</sub> (eÅ <sup>-3</sup> )	0.262; - 0.277

## S2 Details on theoretical calculations

### S2.1 Optimization of crystalline ZNATH by various programs

*Computational details.* VASP: plane-wave basis set with a cutoff of 400 eV, PBE functional, PAW pseudopotentials; CRYSTAL: periodic basis set constructed on the basis of the 6-31G(d,p) atom-centered basis set; B3LYP functional; CPMD: plane-wave basis set with a cutoff of 80 Ry, BLYP functional, Trouiller-Martins pseudopotentials.

*Results.* Selected geometry parameters are listed in Tables S2.1. – S2.3. It can be seen that the agreement between the employed computational methodologies as well as with the experimental structure determination is very good.

**Table S2.1.** Calculated and measured bond lengths in the nitranilate anion. Symmetry operator:  $i) -x, 1 - y, 1 - z$ .

	VASP	CRYSTAL	CPMD	EXP. 100 K
C1 – C2	1.552	1.558	1.558	1.556(2)
C2 – C3	1.421	1.423	1.417	1.415(2)
C1 – C3 <sup><i>i</i></sup>	1.439	1.439	1.439	1.434(2)
C1 – O1	1.240	1.232	1.238	1.2211(18)
C2 – O2	1.255	1.244	1.255	1.2386(18)
C3 – N1	1.431	1.427	1.442	1.4369(18)
N1 – O3	1.256	1.246	1.259	1.2424(17)
N1 – O4	1.245	1.234	1.244	1.2283(17)

**Table S2.2.** Calculated and measured geometric parameters of the H-bonds involving the Zundel cation.

		$D-H / \text{\AA}$	$H \cdots A / \text{\AA}$	$D \cdots A / \text{\AA}$	$D-H \cdots A / ^\circ$	Symm. op. on $A$
O5 $\cdots$ H1 $\cdots$ O6	VASP	1.18	1.25	2.424	175.4	$x, y, z$
	CRYSTAL	1.19	1.22	2.404	174.9	$x, y, z$
	CPMD	1.14	1.30	2.439	175.8	$x, y, z$
	EXP. 100	1.14(4)	1.30(4)	2.4333(16)	174(4)	$x, y, z$
	K					
O5–H5A $\cdots$ O2	VASP	1.00	1.72	2.693	165	$-x, 1-y, 2-z$
	CRYSTAL	0.99	1.77	2.730	165	$-x, 1-y, 2-z$
	CPMD	1.00	1.70	2.682	165	$-x, 1-y, 2-z$
	EXP. 100	0.92(2)	1.82(2)	2.7049(17)	161(2)	$-x, 1-y, 2-z$
	K					
O5B–H5B $\cdots$ O2	VASP	1.00	1.74	2.718	162	$x, y, z$
	CRYSTAL	0.99	1.81	2.765	160	$x, y, z$
	CPMD	1.00	1.76	2.729	161	$x, y, z$
	EXP. 100	0.93(2)	1.80(2)	2.7147(15)	161(2)	$x, y, z$
	K					
O6–H6A $\cdots$ O7	VASP	1.00	1.73	2.730	172	$1+x, y, z$
	CRYSTAL	0.99	1.73	2.718	172	$1+x, y, z$
	CPMD	1.00	1.74	2.744	172	$1+x, y, z$
	EXP. 100	0.93(2)	1.85(2)	2.7734(16)	175(2)	$1+x, y, z$
	K					
O6–H6B $\cdots$ O7	VASP	1.00	1.78	2.775	176	$1+x, 3/2-y, 1/2+z$
	CRYSTAL	0.99	1.76	2.751	176	$1+x, 3/2-y, 1/2+z$
	CPMD	1.00	1.78	2.781	172	$1+x, 3/2-y, 1/2+z$
	EXP. 100	0.93(2)	1.85(2)	2.7734(16)	175(2)	$1+x, 3/2-y, 1/2+z$
	K					

**Table S2.3.** Calculated and measured geometric parameters of H-bonds not involving the Zundel cation.

		$D-H / \text{\AA}$	$H \cdots A / \text{\AA}$	$D \cdots A / \text{\AA}$	$D-H \cdots A / ^\circ$	Symm. op. on $A$
O7–H7A $\cdots$ O1	VASP	0.99	1.96	2.911	160	$x, y, z$
	CRYSTAL	0.98	1.96	2.899	160	$x, y, z$
	CPMD	0.99	1.96	2.911	161	$x, y, z$
	EXP. 100	0.92(2)	2.04(2)	2.9214(15)	161(2)	$x, y, z$
	K					
O7–H7A $\cdots$ O4	VASP	0.99	2.16	2.798	121	$-x, 1-y, 1-z$
	CRYSTAL	0.98	2.16	2.776	120	$-x, 1-y, 1-z$
	CPMD	0.99	2.16	2.784	119	$-x, 1-y, 1-z$
	EXP. 100	0.92(2)	2.21(3)	2.8085(16)	122(2)	$-x, 1-y, 1-z$
	K					
O7–H7B $\cdots$ O3	VASP	0.99	1.97	2.930	164	$-x, 1/2+y, 3/2-z$
	CRYSTAL	0.98	1.92	2.881	165	$-x, 1/2+y, 3/2-z$
	CPMD	0.99	1.93	2.900	165	$-x, 1/2+y, 3/2-z$
	EXP. 100	0.94(3)	2.05(3)	2.9517(14)	159(3)	$-x, 1/2+y, 3/2-z$
	K					
O7–H7B $\cdots$ O4	VASP	0.99	2.40	3.050	123	$-x, 1/2+y, 3/2-z$
	CRYSTAL	0.98	2.39	3.015	165	$-x, 1/2+y, 3/2-z$
	CPMD	0.99	2.42	3.050	121	$-x, 1/2+y, 3/2-z$
	EXP. 100	0.94(3)	2.41(3)	3.0463(15)	125(2)	$-x, 1/2+y, 3/2-z$
	K					



## S2.2 Optimization of substituted analogs of ZNATH in the solid state

*Computational details.* Four analogs of ZNATH were constructed on the basis of the X-ray crystallographic structure data of ZNATH measured at 100 K. The nitro groups were replaced by the following series of functional groups: Cl, H, CH<sub>3</sub> and N(CH<sub>3</sub>)<sub>2</sub>; the unit cell parameters were kept unchanged (Figure S2.2.1). Optimization of analogs imposing periodicity and symmetry constraints was performed by the CPMD program using the BYLP functional and Trouiller-Martins atomic pseudopotentials in conjunction with a plane-wave basis set with the cutoff of 80 Ry. Stability of both tautomeric forms (i.e. with and without the Zundel cation) was examined for each analog by accordingly placing the corresponding hydrogen atoms at the beginning of optimization.

*Results.* Selected geometry parameters and relative stabilities of tautomers (when applicable) of the optimized analogs are listed in Table SJ1. Evidently, on replacing of the nitro group with a less electronegative substituent, the acid remains deprotonated, but the Zundel cation disintegrates to an H<sub>3</sub>O<sup>+</sup>...H<sub>2</sub>O pair. For R=H and R=CH<sub>3</sub> both the structure with and without the Zundel cation exist, the latter resulting from migration of the proton from the H<sub>3</sub>O<sup>+</sup>...H<sub>2</sub>O pair to the acid; energy difference of the tautomers is small. For R=N(CH<sub>3</sub>)<sub>2</sub> only the non-Zundel type of a structure is stable. The gradual disintegration of the Zundel ion on the decreasing electronegativity of R is well reflected in the listed geometry parameters.

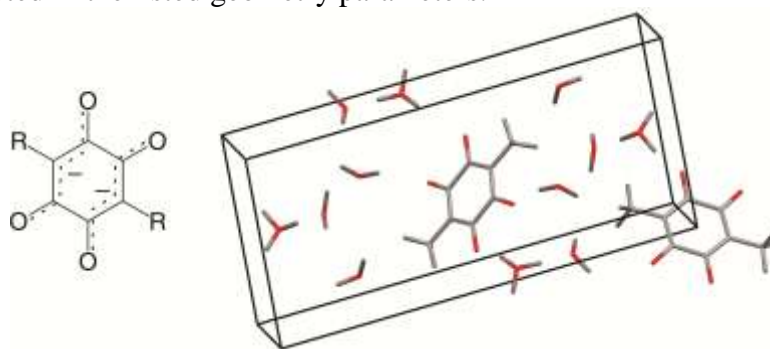


**Figure S2.1.** Left: general scheme of substituted quinoid dianions; right: structure of the methyl analog (R = CH<sub>3</sub>) of ZNATH optimized in the same unit cell as the original compound.

**Table S2.4.** Optimized geometric parameters of H-bonds of ZNATH and its substitution analogs. For analogs with stable structures both with and without the Zundel cation the relative energies of the tautomers are also listed.

R	type	selected atomic distances [Å]				E [kcal/mol]
		O5...O6	O5...H1	O6...H1	O5...O2	
NO <sub>2</sub>	Zundel	2.439	1.142	1.298	2.729	—
Cl	Zundel	2.500	1.070	1.433	2.613	—
H	Zundel	2.581	1.042	1.541	2.571	0.00
	non-Zundel	2.739	1.006	1.733	2.494	0.48
CH <sub>3</sub>	Zundel	2.555	1.043	1.515	2.519	0.00
	non-Zundel	2.711	1.008	1.704	2.478	0.87
N(CH <sub>3</sub> ) <sub>2</sub>	non-Zundel	2.764	0.989	1.777	2.530	—

### S2.3 Structure, NBO analysis and proton affinity of NA analogs (dianions) in the gas phase

*Computational details.* Isolated dianions of the analogs presented in Figure S2.2.1 were optimized in the gas phase at the B3LYP/6-31++G(d,p) level of theory and their electron density was analyzed by the NBO method, as implemented in Gaussian 09. The protonated entities were also optimized in order to compute proton affinities.

*Results.* The bond-antibond stabilization energies of NB orbitals calculated by the second order perturbation approach yield information on effects associated with electron delocalization. Two such effects are indicative for the purpose of this work and displayed in Table S2.5: (i) delocalization of lone electron pair on C3 into the vacant antibond orbital of the C1-O1 bond, and (ii) delocalization of lone pair on O1 into the C1-C2 and C2-C3 antibond orbitals. The former is indicative of the weakening (and thus elongation) of the C1-O1 bond (note that for the free anion C2-O2 and C1-O1 bonds are equivalent), while the latter reflects the tendency of reverse electron delocalization from O2 to the ring and further to the functional group R. The listed values show that the interaction between the lone pair orbital on C3 and the C1-O1 antibond orbital increases in the following order:  $\text{NO}_2 < \text{Cl} < \text{N}(\text{CH}_3)_2 < \text{H} < \text{CH}_3$ ; the trend in the optimized C1-O1 distance (Table S2.5) fairly follows this. Delocalization of the O1 lone pair electrons into the ring increases in the order  $\text{N}(\text{CH}_3)_2 < \text{CH}_3 < \text{H} < \text{Cl} < \text{NO}_2$ , clearly reflecting the increasing electron accepting ability of the functional groups. In line with this is the trend in atomic charge of O1, which decreases with the increasing electron affinity of R (Table S2.5), suggesting the increasing stability of the anion. Finally, the computed proton affinities of the substituted dianions support the increasing acidity of the protonated species (and increasing stability of the dianion) in the following order:  $\text{N}(\text{CH}_3)_2 < \text{CH}_3 < \text{H} \ll \text{Cl} \ll \text{NO}_2$  (Table SJ2). The gas-phase proton affinities are probably insufficient for quantitative assessment of relative acidity in the studied series, particularly considering the condensed phase environment, but it is clear that the high acidity/proton donating ability of nitranilic acid – at least relative to its substitution analogs – is confirmed by all the applied criteria.

**Table S2.5.** B3LYP/6-31++G(d,p) calculated bond-antibond interaction energies of the selected NB orbitals, optimized C-O distances, NBO atomic charge on O1 and proton affinity (per one proton) for the various substitution analogs of the quinoid dianion. All quantities were computed using isolated models.

property	ring substituent R (on C3, see Figure S2.1)				
	N(CH <sub>3</sub> ) <sub>2</sub>	CH <sub>3</sub>	H	Cl	NO <sub>2</sub>
<b>NBO interactions [kcal/mol]</b>					
LP(C3) → BD*(C1-O1)	102.75	129.00	117.12	100.20	92.72
LP(O1) → BD*(C2-C3)	14.24	14.18	13.63	16.02	17.82
LP(O1) → BD*(C1-C2)	19.90	20.54	21.17	22.84	23.01
<b>other properties</b>					
C1-O1 distance [Å]	1.259	1.261	1.260	1.246	1.237
NBO charge of O1	-0.709	-0.720	-0.722	-0.672	-0.625
Proton affinity [kcal/mol]	383.6	380.1	378.0	364.2	346.0

## S2.4 First-principle calculations of isotropic chemical shifts

*Computational details.* First-principles calculations were performed using the density functional theory in the generalized gradient approximation of Perdew-Burke-Ernzerhof (GGA PBE) with plane wave basis and ultra-soft pseudopotentials, as implemented in the CASTEP package (Accelrys). The plane-wave cutoff energies were 700 eV, the reciprocal-space sampling was performed with the *k*-point grid of 8×2×3 points. All-electron information, needed for the calculation of NMR observables, was reconstructed using the GIPAW method as implemented in NMR CASTEP module. The module yielded chemical shielding tensors, but only <sup>1</sup>H isotropic chemical shifts, extracted from the corresponding shielding tensors, were compared to experimentally determined values. In experiments, the <sup>1</sup>H isotropic chemical shift is reported relative to a selected reference signal; for <sup>1</sup>H nuclei the reference signal is usually the signal of tetramethylsilane. Differently, the parameters obtained directly from calculations are the ‘absolute’ isotropic shielding parameters (a third of the trace of the shielding tensors). In order to compare these parameters for different carbon and proton sites to corresponding experimental chemical shifts, we determined  $\sigma_{ref}^{iso}$  with the help of the expression

$$\delta_{calc}^{iso} = \sigma_{ref}^{iso} - a\sigma_{calc}^{iso}$$

so that the agreement between the calculated and the measured chemical shifts was the best. Here  $\sigma_{calc}^{iso}$  is the calculated isotropic shielding parameter. Note that the calculations and measurements agreed better if a small deviation from 1 was allowed for the scaling factor *a*.

The isotropic chemical shifts were calculated based on the original structural model as obtained from the diffraction data, as well as based on the structural models in which either positions of hydrogen atoms or positions of all atoms within the structure were optimized using the DFT calculations. The agreement between the measured and the calculated values of isotropic chemical shifts was the best for the structural model with optimized positions of hydrogen nuclei. The agreement was only slightly worse for the original structural model.

### S3 Spectroscopic characteristics of the nitranilate anion

#### S3.1 Infrared spectroscopy

*IR spectrum of sodium salt of NA.*

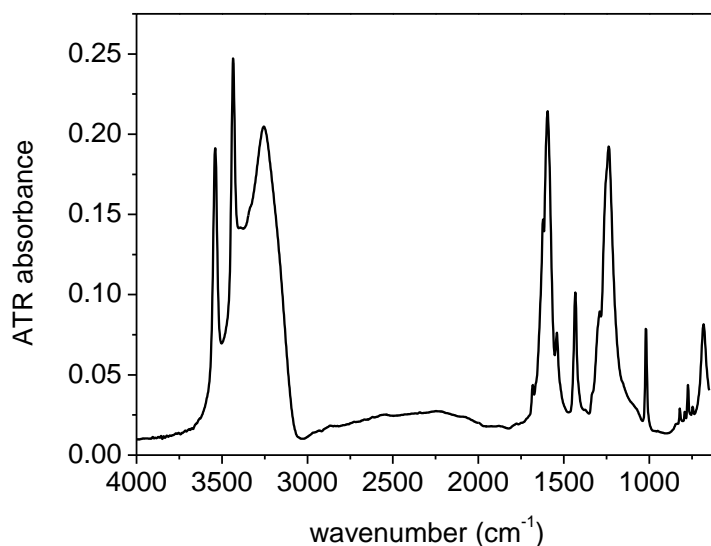


**Figure S3.1.** Corrected ATR spectrum of hydrated sodium salt of NA.

*Low temperature IR spectrum.* The cooling of the crystalline ZNATH red shifts bands due to OH stretching with concomitant reductions of the band halfwidth. The most significant is the red shift of the central OH stretching band which monotonically shifts to approximately  $3000\text{ cm}^{-1}$  at 128 K (Figure S3.2). The increase of the intensity at low wavenumbers suggests that is similar red frequency shift accompanied by the  $\text{O}\cdots\text{H}\cdots\text{O}$  stretching of Zundel cation; however, the exact maximum of the shifted band is screened with overlapped bands of NA.

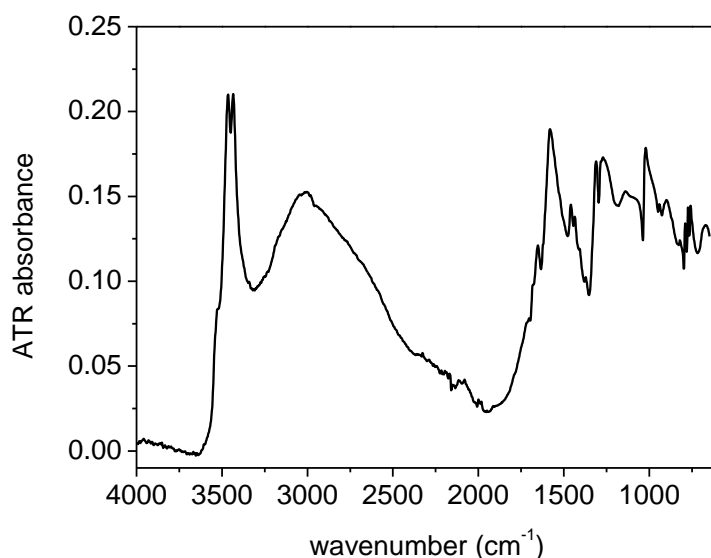


**Figure S3.2.** Corrected ATR spectrum of ZNATH at 128 K.

### S3.2 Raman spectroscopy

Tiny crystals of ZNATH were placed on a microscope slide of micro Raman accessory of the T64000 Horiba-JobinYvon Raman spectrometer with CCD detector, operating in micro single mode with 50x objective. Green 514.5 nm laser line of COHERENT INNOVA 400 argon ion laser with power of 0.3 mW on the sample served as an excitation source. Laser power reduction was obtained with two attenuators. Spectra in the region 100 - 1800  $\text{cm}^{-1}$  were collected in multiwindows mode with time constant of 10 s and four accumulations. Phonon spectra down to 10  $\text{cm}^{-1}$  were recorded in a single window micro-triple mode using gratings having 1800 grooves/mm.

Green laser light proved to initiate a photochemical reaction of ZNATH in cases when laser power was greater or equal 0.9 mW. An attention was paid to inspect the crystallite images before and after Raman spectra were recorded. In Figure S3.3. is shown a comparison between: a) intact, unaffected crystal and b) a product of a photoreaction. While the original crystallite is yellowish and transparent, the photoreaction product forms white polycrystalline powder. Raman spectrum of ZNATH is presented in Figure S3.4.

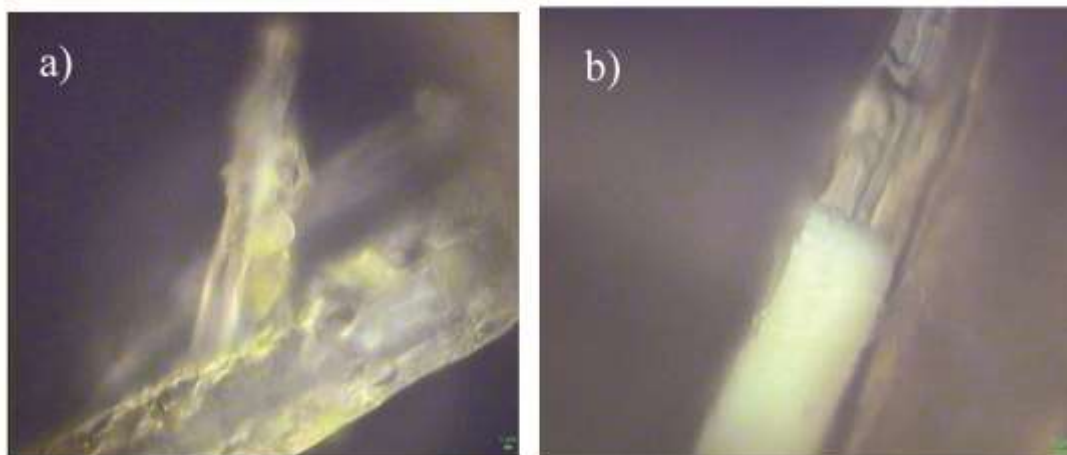


**Figure S3.3.** Left: (a) intact microcrystals of ZNATH, right: (b) same microcrystals after irradiation with 514.5 nm laser light.

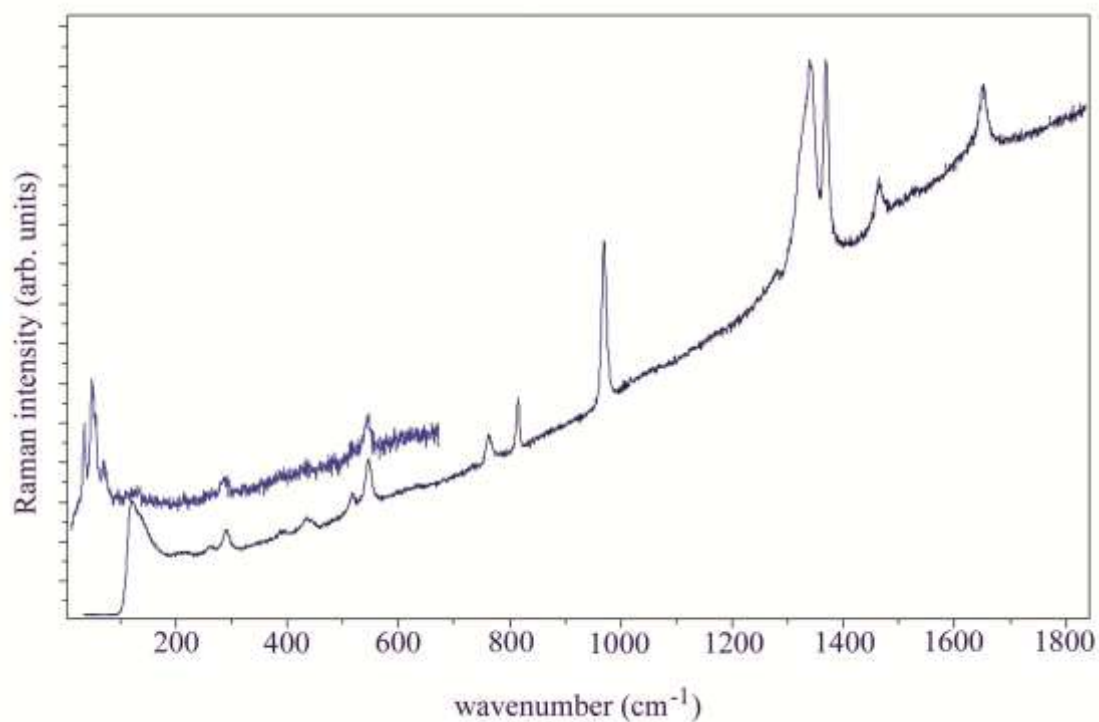


**Figure S3.4.** Raman spectra of ZNATH (10 - 1800  $\text{cm}^{-1}$ ). Laser power 0.3 mW.

No vibration in Raman spectrum could be confidently assigned to the Zundel cation. Most intensive Raman bands correspond to the stretching mode of carbonyl groups ( $1652 \text{ cm}^{-1}$ ),  $\text{NO}_2$  symmetric stretching modes combined with C-C stretching ( $1369$  and  $1340 \text{ cm}^{-1}$ ), C-N stretching modes combined with  $\text{NO}_2$  bending, and C-C ring stretching ( $970 \text{ cm}^{-1}$ ), while weaker bands correspond to  $\text{NO}_2$  out of plane ( $815 \text{ cm}^{-1}$ ) and in plane ( $762 \text{ cm}^{-1}$ ) bending, C-N-O bending ( $547 \text{ cm}^{-1}$ ), C-C=O bending ( $436 \text{ cm}^{-1}$ ) and C-C-C in plane bending ( $290 \text{ cm}^{-1}$ ). List of all observed bands is given in table S3.1.

The bending band of water which commonly occurs at  $1643 \text{ cm}^{-1}$  is overlapped by much stronger carbonyl stretching band at  $1652 \text{ cm}^{-1}$ . The weak band

at  $1280\text{ cm}^{-1}$  might originate from C-O stretching and C-O-H bending modes of undissociated NA.

At least three internal modes of NA are expected below  $150\text{ cm}^{-1}$  in the region of lattice vibrations. Since the number of NA molecules in the elementary cell is two, and the space group is  $P2_1/c$ , for them we expect  $2 A_g + 4 B_g + 2 A_u + B_u$  lattice optical phonons. Six water molecules contribute three translations and three rotations each, but these modes are notoriously weak in Raman spectrum.

**Table S3.1.** Observed bands with approximative assignment of ZNATH<sup>†</sup>.

observed (cm <sup>-1</sup> )	descriptive assignment
1652 m	$\nu(\text{C}=\text{O})$
1528 w	$\nu(\text{C}=\text{C})$
1465 m	$\nu_{\text{asym}}(\text{NO}_2)$ asymmetric NO <sub>2</sub> stretching
1369 s	$\nu_{\text{sym}}(\text{NO}_2) + \nu(\text{C}-\text{C})$ symmetric NO <sub>2</sub> stretching
1340 s	$\nu_{\text{sym}}(\text{NO}_2) + \nu(\text{C}-\text{C})$
1331 s,sh	$\nu(\text{C}-\text{N}) + \nu(\text{NO}_2)$
1322 m,sh	$\nu(\text{C}-\text{N}) + \nu(\text{NO}_2)$ ,
1280 w	$\nu(\text{C}-\text{C}) + \delta(\text{COH})$ undissociated NA
970 s	$\nu(\text{C}-\text{C}) + \nu(\text{C}-\text{N})$ ring breathing
815 m	$\lambda(\text{NO}_2)$ out of plane deformation
762 m	$\delta(\text{O}-\text{N}-\text{O})$ in plane NO <sub>2</sub> bending
547 m	out of plane ring deformation
518 w	$\delta(\text{C}-\text{C}-\text{C})$ in plane bending
436 w	$\delta(\text{O}=\text{C}-\text{C})$ in plane bending
392 vw	$\delta(\text{C}-\text{C}-\text{C})$ in plane bending
290 mw	$\delta(\text{C}-\text{C}-\text{C})$ in plane bending
261 w	$\delta(\text{C}=\text{C}-\text{N})$ in plane bending
215 vw	out of plane ring deformation
128 w	$\tau(\text{NO}_2)$ in phase
72 mw	lattice vibration, libration of NA
55 m,sh	lattice vibration, libration of NA
50 s	lattice vibration, libration of NA
34 m	lattice vibration, translation of NA

<sup>†</sup>s-strong, m-medium, w-weak, sh-shoulder